Research Square

Preprints are preliminary reports that have not undergone peer review.
They should not be considered conclusive, used to inform clinical practice,
or referenced by the media as validated information.

Post-Processing Strategies for Generative Design Outcomes in a UAV Tail Boom

Michał Piotr Kowalik

michal.kowalik@pw.edu.pl

Warsaw University of Technology: Politechnika Warszawska https://orcid.org/0000-0002-7632-6782

Piotr Stapiński

Mateusz Papis

Research Article

Keywords: generative design, fused deposition modeling, post-processing, design for additive manufacturing, UAV structures

Posted Date: May 28th, 2026

DOI: https://doi.org/10.21203/rs.3.rs-9543342/v1

License: This work is licensed under a Creative Commons Attribution 4.0 International License.
Read Full License

Post-Processing Strategies for Generative Design Outcomes in a UAV Tail Boom

Michał Kowalik [1*], Piotr Stapiński [2] and Mateusz Papis [1]

[1]Warsaw University of Technology, Institute of Aeronautics and Applied Mechanics, Poland.
[2]Łukasiewicz Research Network – Institute of Aviation, Poland.

*Corresponding author(s). E-mail(s): michal.kowalik@pw.edu.pl;
Contributing authors: piotr.stapinski@ilot.lukasiewicz.gov.pl; mateusz.papis@pw.edu.pl;

Abstract

Generative design produces structurally efficient but organically shaped geometries that require post-processing before Fused Deposition Modeling (FDM) manufacturing. This paper compares two post-processing strategies applied to the same generative design outcome for an Unmanned Aerial Vehicle (UAV) tail boom: a complex variant faithful to the raw topology, and a simplified variant with symmetric arms, self-supporting geometry, and uniform cross-sections oriented toward FDM manufacturability. Both variants were evaluated using linear static and buckling finite element analysis under identical loading conditions. Scaled prototypes of the simplified variant were FDM-printed at two infill configurations and physically load-tested. The manufacturing-oriented simplification reduced both mass and print time while eliminating support structures; peak stress remained well below the material limit. FEA-predicted stress concentrations correlated with observed fracture locations in physical tests. For lightly loaded polymer FDM structures, these results suggest that manufacturing-oriented simplification of generative design outcomes incurs a negligible structural penalty while improving printability and reducing production cost.

Keywords: generative design, fused deposition modeling, post-processing, design for additive manufacturing, UAV structures

1 Introduction

Additive manufacturing (AM) offers broad geometric freedom, allowing designers to place material only where structurally required. Topology optimization and generative design exploit this freedom to create lightweight, load-adapted structures that would be impractical or cost-prohibitive through conventional methods [1, 2]. The aerospace and Unmanned Aerial Vehicle (UAV) sectors have adopted these approaches early: Airbus achieved a 45% weight reduction on an A320 cabin partition using generative design [3], and GE Aerospace consolidated over 100 parts into a single unit [4]. Generative design is now increasingly accessible through commercial CAD platforms [5, 6].

Despite these advances, raw generative design and topology optimization outputs are not

directly manufacturable. The organic shapes produced by these methods typically contain thin features, unsupported overhangs, and abrupt geometry transitions that violate manufacturing constraints [1, 7]. Reconstruction of optimized topologies into manufacturable CAD geometry has been identified as a "striking challenge" [7] and the most time-consuming step in the optimization-to-manufacturing workflow [2, 8]. A similar usability gap exists for deep generative models, where generated designs require conversion to manufacturable formats [9]. The reconstruction process is inherently lossy: structural performance degrades during manual translation from optimized mesh to parametric CAD [5, 10]. Langelaar [10] demonstrated that embedding additive manufacturing constraints directly into topology optimization can reduce this loss, but such formulations are not yet standard in commercial generative design tools.

Generative design has demonstrated advantages over conventional topology optimization partly because topology optimization requires more extensive post-optimization reconstruction. Barbieri and Muzzupappa [5] showed that generative design outperformed topology optimization on both a rocker arm and a brake pedal, attributing part of the advantage to the lossy reconstruction step. However, existing evaluation methodologies focus on selection criteria — mass, stress, displacement, safety factor — without addressing how the selected output should be translated into a final manufacturable design [11]. Design for Additive Manufacturing (DfAM) frameworks such as Generative Design for Additive Manufacturing (G-DfAM) [6] recognize a "refinement phase" between raw optimization output and manufacturing-ready geometry, but treat this phase qualitatively rather than quantitatively [12].

Generative design has been applied across several UAV application domains with encouraging results. In frame and chassis optimization, Balayan et al. [13] used Fusion 360 generative design to redesign a quadcopter chassis, achieving approximately 50% weight reduction, while Kowalik et al. [14] combined topology optimization and generative design for drone frame optimization, demonstrating their complementary strengths. In aerodynamic component design, Maisto et al. [15] applied iterative generative design with DfAM constraints to a UAV vertical tail, reducing mass by 71.2% compared to a metallic benchmark. In multi-method approaches, Zhang et al. [8] combined generative design with subsequent topology optimization refinement for a biped robot component, explicitly identifying the reconstruction step as the most time-consuming part of the workflow. However, most of these studies stop at finite element analysis without physical validation, including generative design studies for aerospace [11] and UAV components [13, 15]. The few studies that include physical testing tend to use metal AM processes such as Selective Laser Sintering (SLS) and laser powder bed fusion rather than polymer FDM [16], or employ conventional design methods without generative design [17].

Fused Deposition Modeling (FDM) introduces process-specific constraints distinct from metal AM. Build orientation and layer adhesion create significant anisotropy, reducing tensile strength by up to 75% in upright orientation compared to flat orientation for PLA [18]. Finite element (FE) models ignoring fabrication-angle-dependent anisotropy significantly overestimate structural performance [19]. Infill density dominates mechanical behavior: density governs tensile strength (100% rectilinear ABS: 36.4 MPa vs. 20%: 16 MPa), while pattern type causes less than 5% variation at equivalent densities [20]. Honeycomb and grid patterns achieve comparable strength to solid infill at lower weight [21]. Deposition path direction and build orientation significantly affect topology-optimized FDM parts [22]. These process-specific effects mean that post-processing of generative design outputs for FDM must address printability, support elimination, and orientation-dependent strength [23].

Despite this body of knowledge, no study has systematically compared how post-processing fidelity — the degree to which the final design follows the raw generative design output — affects both structural performance and FDM manufacturing outcomes with physical validation. Existing work either optimizes geometry without considering additive manufacturing constraints, stopping at FEA [8, 11] — a pattern consistent across UAV applications [13, 15] and generative design for AM studies [24] — or considers additive manufacturing constraints without evaluating the structural cost of simplification [12, 25]. The present paper provides quantitative evidence from both simulation and physical testing to evaluate this trade-off. Two

post-processing strategies — one faithful to the raw generative design output, the other oriented toward FDM manufacturability — were applied to the tail boom of an unmanned helicopter platform. Both were analyzed with FEA and the simplified variant was prototyped and load-tested to assess whether manufacturing-oriented simplification is structurally justified.

The paper first describes the case study platform, design loads, and generative design setup, then presents the two post-processing strategies and FEA methodology, followed by prototype fabrication and physical testing results, and concludes with a discussion of implications and limitations.

2 Case Study and Generative Design Setup

2.1 UAV Platform and Design Requirements

The case study component is the tail boom of ARCHER (Autonomous Reconfigurable Compound Helicopter for Education and Research), a modular unmanned helicopter platform developed at Warsaw University of Technology [26, 27]. Figure 1 shows the ARCHER platform with the tail boom structure indicated. Table 1 summarizes the platform specifications. Platform parameters are drawn from [26], the published energy analysis [27], and internal platform documentation.

Table 1 ARCHER platform specifications

Parameter	Value	Unit
Main rotor diameter	1.78	m
Main rotor blades	2	—
Main rotor speed (nominal)	1100	RPM
Tail rotor diameter	0.316	m
Tail rotor speed	9000	RPM
Maximum take-off weight	12.5	kg
Propulsion	Electric	—
Rotor head type	Rigid	—

The ARCHER features a frame fuselage with carbon fiber composite plates and a modular architecture supporting optional configurations including wings with propellers and a pusher rotor. The original tail boom is a carbon fiber composite tube (22 mm outer diameter) providing a structural link between the fuselage and the tail rotor assembly with sufficient moment arm to balance main rotor torque. The design objective was to create an alternative tail boom manufacturable via FDM, accepting a weight penalty in exchange for manufacturing accessibility, cost reduction, and rapid design iteration capability. The structure was designed to withstand loads from all optional elements, including the pusher rotor.

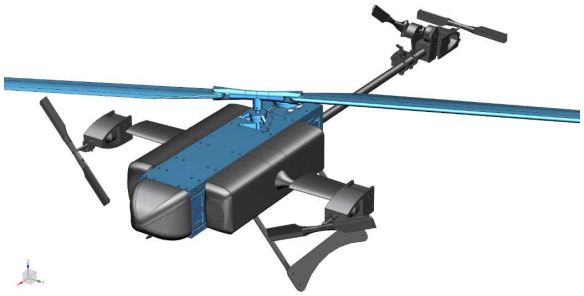


Fig. 1 The ARCHER unmanned helicopter platform with modular tail boom structure indicated

2.2 Load Cases

Four force components act on the tail boom: tail rotor thrust, forward-flight aerodynamic drag, cross-flow drag, and gravity. The tail rotor thrust required to balance the main rotor torque is:

$$T_{TR} = \frac{P_{MR}/\omega_{MR}}{d_{MR\text{-}TR}} \tag{1}$$

where P_{MR} is main rotor power, ω_{MR} is main rotor angular velocity (in rad/s), and $d_{MR\text{-}TR}$ is the distance from the main rotor axis to the tail rotor. The aerodynamic drag forces are:

$$D = \tfrac{1}{2}\, C_D\, \rho\, V^2\, A \tag{2}$$

where C_D is the drag coefficient, ρ is air density, V is the airspeed, and A is the projected area. Equation (2) is applied separately for forward-flight drag and cross-flow drag. The gravitational force on the tail assembly is 6.84 N, computed from the tail element mass (0.697 kg).

Table 2 lists the input parameters used in load calculation.

Table 2 Input parameters for load calculation

Parameter	Symbol	Value	Unit
Main rotor power	P_{MR}	1000	W
Main rotor rotational speed	ω_{MR}	1000	RPM
Main rotor–tail rotor dist.	$d_{MR\text{-}TR}$	0.96	m
Drag coefficient	C_D	1.15	—
Air density	ρ	1.225	kg/m^3
Forward velocity	V_{fwd}	55.56	m/s
Cross-flow velocity	V_{cross}	10	m/s
Tail elements mass	m_{tail}	0.697	kg

Source data: [26–28] and internal platform documentation.

The resulting forces are: $T_{TR} = 9.95$ N, $D_{aft} = 14.47$ N, $D_{cross} = 1.557$ N, and $F_g = 6.84$ N.

Several assumptions were deliberately conservative. The main rotor speed used in load calculation (1000 RPM) was rounded down from the nominal value (1100 RPM, Table 1), which increases the computed torque and thus yields a higher tail rotor thrust estimate. The forward velocity of 200 km/h provides a large margin over comparable platforms (100–120 km/h). The flat-plate drag coefficient ($C_D = 1.15$) overestimates drag on streamlined tail components [28]. The motor efficiency was set to 100%, further increasing the tail rotor thrust above realistic values.

Figure 2 illustrates the two load cases. They differ only in the direction of the lateral crosswind and the corresponding tail rotor thrust direction: Load Case 1 applies rightward thrust and rightward cross-flow drag, while Load Case 2 reverses both. All forces were applied simultaneously in both generative design and subsequent FEA. Boundary conditions consisted of fixed supports (all degrees of freedom constrained) at four M4 bolt holes at the fuselage attachment interface.

2.3 Material Selection

Three common FDM filament materials were evaluated: PLA, ABS, and PETG. Table 3 summarizes the comparison.

ABS was selected for three reasons. First, its heat deflection temperature (98°C) provides adequate thermal resistance for outdoor UAV operations, whereas PLA (∼55°C) and PETG (∼70°C) risk softening in direct sunlight. Second, ABS has the lowest density (1.04 g/cm^3), yielding a higher strength-to-weight ratio at equivalent geometry.

Table 3 Material properties comparison for FDM filament candidates

Property	PLA	ABS	PETG
Tensile str., 100% hex [MPa]	49.82	—[a]	49.05
Tensile str., 50% hex [MPa]	42.23	42.54	45.66
Flexural str., 100% hex [MPa]	101.02	83.67	72.54
Impact str., 100% hex [kJ/m^2]	0.226	1.136	0.21
Heat defl. temp. [°C]	∼55	∼98	∼70
Density [g/cm^3]	1.24	1.04	1.27

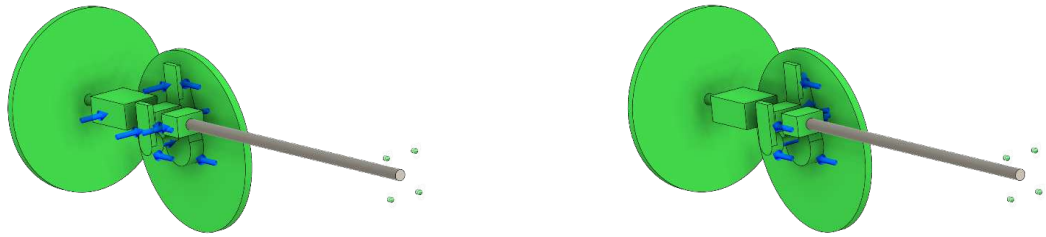
Source data compiled from manufacturer datasheets and material testing reports [29]. [a] Value omitted; original ABS data at 100% honeycomb infill is inconsistent across sources.

Third, ABS exhibits the highest impact strength among the three candidates, relevant for landing loads and potential impacts.

For FEA, material properties were taken from the worst-case (vertical/upright) print orientation as characterized by Zou et al. [30]: Young's modulus $E = 2399.7$ MPa, Poisson's ratio $\nu = 0.37$, shear modulus $G = 875.5$ MPa, and ultimate tensile strength $\sigma_{UTS} = 25.75$ MPa. This conservative approach accounts for complex generative design geometries containing surfaces at various angles relative to the build plate. The prototypes described in Section 4 were printed in PLA+ for practical reasons; this material mismatch is addressed in Section 6.3.

2.4 Generative Design Configuration and Parametric Exploration

Generative design was performed in Autodesk Fusion 360 with the objective of maximizing stiffness under a mass constraint. The minimum safety factor for both stress and buckling was set to 1.7. The preserve geometry comprised the tail rotor



(a) (b)

Fig. 2 Load cases applied in generative design and FEA: (a) Load Case 1 with rightward tail rotor thrust, (b) Load Case 2 with leftward tail rotor thrust

assembly (rotor hub, engines, mounting hardware), required for force application. Obstacle geometry defined clearance volumes around rotor elements (Fig. 3).

The resolution was set to 4 mm, the maximum available in Fusion 360. To compensate for the mass discrepancy between the Fusion 360 model of the tail rotor assembly (∼4.2 kg) and the actual hardware (0.697 kg), gravity was disabled and replaced with an equivalent point force of 6.84 N.

A parametric sweep was conducted across 12 mass variants ranging from 4.5 kg to 9.5 kg total (in 0.5 kg steps), plus one run with the minimize-mass objective. The relatively high mass targets were intentional: the dense generative design output was intended to be subsequently lightened by reducing infill density during FDM fabrication, making the solid geometry a starting envelope rather than a final mass target. The topology evolved systematically: the lightest variants produced three-bar truss structures, four main bars appeared above 4.99 kg, bars thickened progressively with increasing mass, and above 7.46 kg the bars merged into oval sections (Fig. 4).

To compare the variants quantitatively, preliminary linear static stress analyses were performed on the generative design outputs with a uniform stress legend of 0–0.5 MPa, following a selection approach similar to that proposed by Dalpadulo et al. [31]. The comparison metrics comprised: stress-to-mass ratio (lower is better), peak Von Mises stress, and visual assessment of stress distribution uniformity across the structure. Table 4 presents results for five representative variants.

Table 4 Generative design parametric exploration results (selected variants)

Total mass [kg]	Boom mass[a] [kg]	Peak stress [MPa]	Stress/mass [MPa/kg]
5.47	1.295	0.57	0.44
6.27	2.096	0.72	0.34
6.97	2.795	0.34	0.12
8.45	4.275	0.20	0.05
9.43	5.255	0.18	0.03

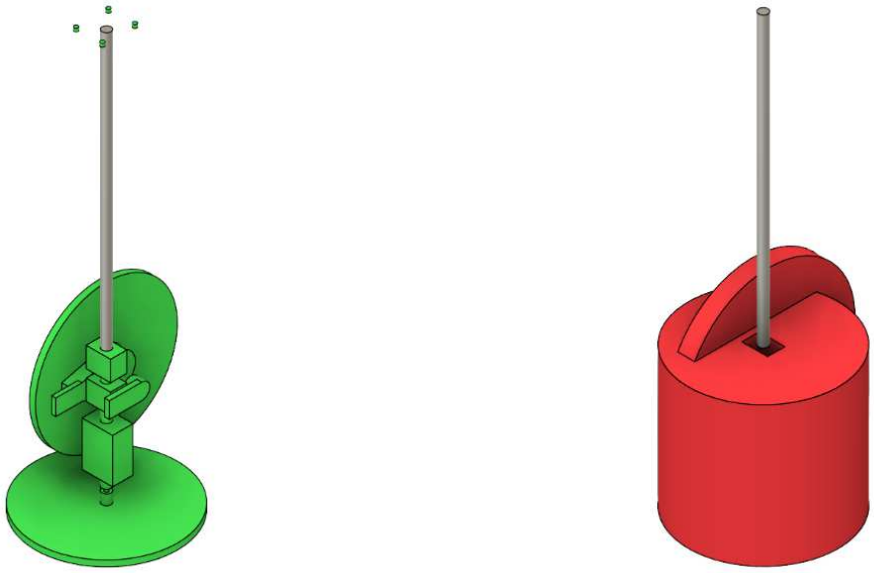
[a] Real boom mass = total model mass minus preserve-geometry components (∼4.2 kg in Fusion 360; actual hardware: 0.697 kg). Compensated as described in Section 2.4.

The 7 kg variant (real boom mass: 2.795 kg) was selected for post-processing. It offered the best balance between low stress (0.34 MPa), a favorable stress-to-mass ratio (0.12), and absence of localized stress concentrations that affected lighter variants. The large margin between peak stress and material strength (safety factor > 75) indicated sufficient reserve to accommodate mass reduction through infill decrease during printing.

3 Post-Processing Strategies and FEA Methodology

3.1 Complex Variant — Generative Design-Faithful Post-Processing

The first strategy aimed to replicate the generative design topology as closely as possible in parametric CAD geometry. The reconstructed model preserved: asymmetric arm cross-sections (the upper arm on the tail rotor side has a larger diameter and is positioned further from the centerline), varying thicknesses along the arms, and original brace positions.



(a) (b)

Fig. 3 Generative Design setup in Fusion 360: (a) preserve geometry, (b) obstacle geometry

Modifications from the raw output were limited to manufacturing necessities: filling small holes, smoothing regions cut by obstacle geometry, adding root fillets, reinforcing the fuselage base, and providing threaded inserts (M4 at fuselage, M8 at tail rotor).

Elliptical splines were used for the supporting braces (Fig. 5). The overall structure at 100% infill had a mass of 3.351 kg. A key manufacturing consequence is that the irregular, asymmetric shape cannot be placed flat on a build plate without generating support structures on the lower arms, creating weak interface layers and rough surfaces.

3.2 Simplified Variant — Manufacturing-Oriented Post-Processing

The second strategy prioritized FDM manufacturability while retaining the generative design-derived load paths. Five key simplifications were applied, each driven by a specific FDM constraint: (1) symmetric main arm placement enabling consistent layer deposition; (2) rectangular upper arm cross-sections with rounded corners providing flat surfaces for direct build-plate contact without supports; (3) uniform brace cross-sections simplifying toolpath generation; (4) an H-shaped fuselage base with taper for stable build plate adhesion; and (5) additional reinforcement near the tail attachment to compensate for the stress concentration at the arm convergence.

The primary manufacturing advantage is that the lower arms can be printed directly on the build plate without support structures, producing smooth bottom surfaces and eliminating the weak support-interface layer (Figs. 6 and 7).

The overall mass at 100% infill was 3.211 kg — 4% lighter than the complex variant.

3.3 FEA Setup

Finite element analysis was performed using Autodesk Fusion 360's Simulation module, selected for its tetrahedral meshing suited to irregular generative design geometries and geometric consistency within the design platform. The material model was isotropic, using the ABS worst-case orientation properties from Section 2.3. By using the weakest orientation properties, the analysis provides a conservative lower bound [18, 19].

Table 5 summarizes the mesh parameters.

Boundary conditions were identical to those used in generative design: fixed supports at the fuselage mounting holes (Fig. 8). Three analysis



(a) (b) (c) (d)

Fig. 4 Evolution of generative design topology with increasing mass constraint: (a) 5.47 kg, (b) 6.97 kg, (c) 8.45 kg, (d) 9.43 kg total mass



Fig. 5 Complex (generative design-faithful) post-processed geometry (dark) overlaid on the raw generative design outcome



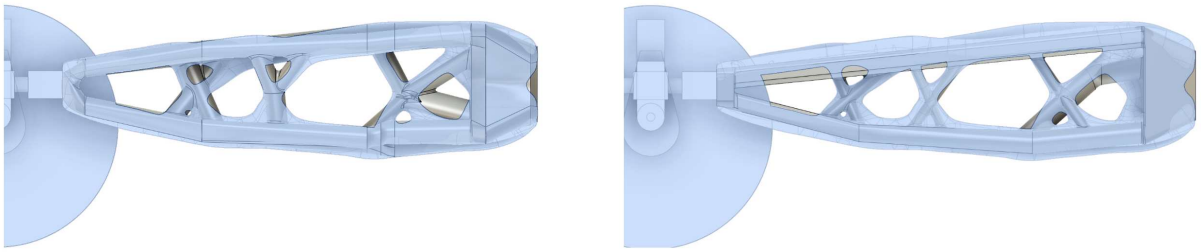
Fig. 6 Simplified (manufacturing-oriented) post-processed geometry (dark) overlaid on the raw generative design outcome

Table 5 FEA mesh parameters

Parameter	Complex	Simplified
Element type	Parabolic tet.	Parabolic tet.
Elements	676,313	788,049
Nodes	1,027,186	1,198,538
Model-based size	1%	2% + local
Element placement	On curved surf.	On curved surf.
Min. element size	10% of avg.	10% of avg.

types were performed for each variant and load case: linear static stress (Von Mises), displacement, and linear buckling (three modes per load case).

A formal mesh convergence study was not performed. Mesh adequacy is supported by three



(a) (b)

Fig. 7 Side view comparison of post-processed variants overlaid on generative design outcome: (a) complex, (b) simplified

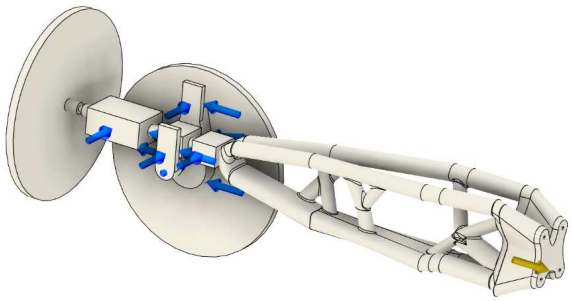


Fig. 8 FEA boundary conditions and applied loads (Load Case 1 shown)

arguments: stress levels are less than 2% of the material UTS, two independent meshes on different geometries produced physically coherent results, and parabolic elements converge faster than linear elements. The absence of a formal convergence study is a limitation acknowledged in Section 6.3.

4 Prototype Fabrication and Physical Testing

4.1 Prototype Printing

Two specimens of the simplified variant were printed at 40% scale on a Bambu Lab P1S printer using Sunlu PLA+ filament for destructive testing. Table 6 summarizes the print parameters and resulting specimen properties.

Mounting holes were adapted for testing: three M3 screws at the fuselage end and one M6 bolt at the tail end for load application. Figure 9 shows the slicer preview and printed specimens.

Table 6 Print parameters and results for 40% scale test specimens (Bambu Lab P1S, Sunlu PLA+)

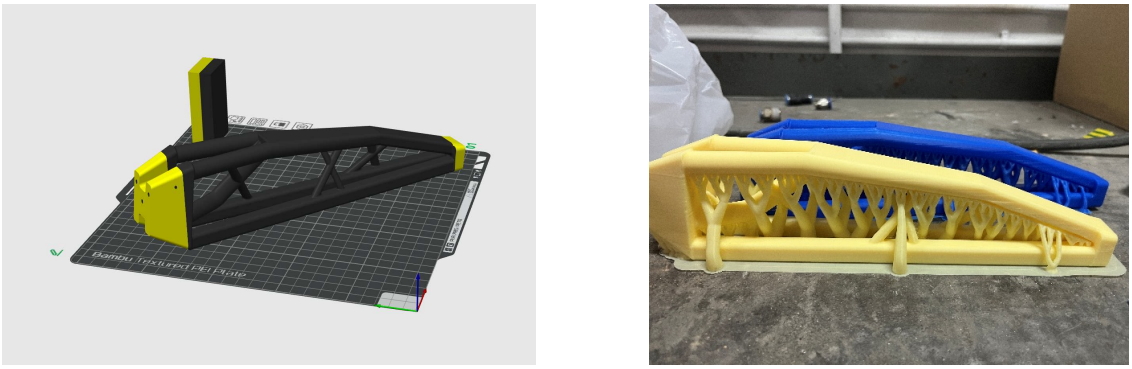
Parameter	Solid	Shell
Nozzle diameter	0.4 mm	0.4 mm
Layer height	0.2 mm	0.2 mm
Infill density	100%	0%
Wall thickness	–	1 mm (2 mm at mount.)
Mass	234 g	106 g
Print time	8 h 12 min	5 h 26 min

4.2 Load Testing

The test setup, shown in Fig. 10, comprised the printed structure mounted on a 19 mm furniture board via three M3 screws and universal adhesive, clamped to a welding fixture table. An M6 bolt at the tail end served as the load application point.

Loading was applied incrementally using dead weights. At each step, the weight was applied and then removed to check for permanent deformation. The solid-infill specimen was loaded in 19 steps up to 18.15 kg. Displacement was minimal (a few millimeters), attributed primarily to deformation of the furniture board as the screws began to pull through at higher loads. At 18.15 kg, the furniture board fractured and separated from the fixture table; the printed structure remained intact. The ultimate capacity of the solid-infill structure was therefore not reached, and 18.15 kg represents a lower bound.

The shell specimen was loaded in 14 steps up to 12.0 kg. Progressive displacement of approximately 10 mm (bending at the loaded end) was observed. At 12.0 kg, the structure failed. Fractures occurred at brace-to-arm junctions and at geometry transitions — precisely the locations where cross-section changes introduce stress concentrations. The failure mode was brittle, consistent with PLA+ behavior under high stress.



(a) (b)

Fig. 9 Test specimens at 40% scale: (a) slicer preview with reinforced regions, (b) printed specimens

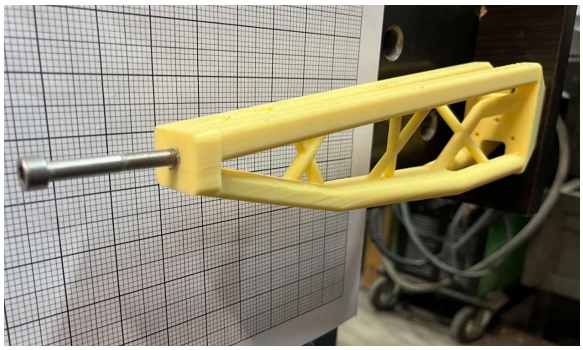


Fig. 10 Physical load testing setup: loading configuration with specimen mounted on fixture board

Figure 11 shows the load test outcomes for both specimens.

FEA correlation with physical test. To compare the numerical model with test observations, FEA was performed on the 40%-scale simplified geometry using PLA+ material properties (published tensile strength: 39.9–52.5 MPa [32]). A load of 117.2 N (12 kg) was applied at the tail bolt location. The FEA produced general stress levels of 2–10 MPa, with peaks of 12.3 MPa on structural members and 21 MPa at mounting holes (the latter likely affected by the idealized boundary condition). The high-stress regions — root fillets at brace connections, geometry transitions, and the fuselage-end mounting area — correlated with observed fracture locations in the shell specimen (Fig. 12). This qualitative correlation follows a similar approach to Yap et al. [16], who demonstrated close agreement between FE predictions and physical tests for an SLS-printed micro-drone. Al-Hadithi et al. [17] employed multi-scenario FEM validation representing a higher level of rigor that future work should aim toward.

5 Results and Comparison

5.1 Structural Performance Comparison

Table 7 compiles the FEA results for both variants under identical conditions (full scale, 100% infill, ABS worst-case properties).

The simplified variant exhibits 31% higher peak Von Mises stress (0.43 vs. 0.32 MPa). In absolute terms, both values are negligible relative to the material limit: less than 2% of the ABS ultimate tensile strength (25.75 MPa), yielding safety factors of approximately 60–80. Peak displacements (0.17 and 0.23 mm) are less than 0.04% of the 700 mm boom length.

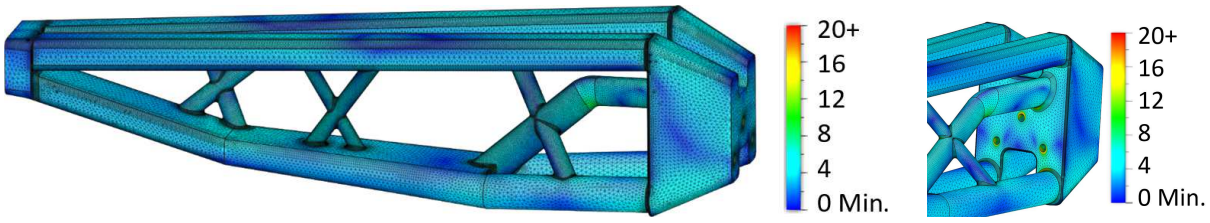
Stress distributions follow similar patterns in both variants (Fig. 13). Under Load Case 1, one upper arm carries the majority of the load; under Load Case 2, both upper arms are stressed. Stress concentrations appear at geometry transitions — brace-arm junctions, arm convergence at the tail end, and the fuselage base — consistent between variants, confirming that the overall load paths established by generative design are preserved in both strategies.

The buckling analysis produced an unexpected result: the simplified variant exhibits superior buckling resistance (eigenvalues 75–266 vs. 43–114). The symmetric, uniform cross-sections distribute compressive loads more evenly, avoiding the localized buckling initiation that can occur in irregular geometry.



(a) (b)

Fig. 11 Load test outcomes: (a) solid-infill specimen at 18.15 kg showing fixture board failure (structure intact), (b) shell specimen after structural failure at 12.0 kg with visible fracture locations



(a) (b)

Fig. 12 FEA validation at test conditions (117.2 N, 40% scale, PLA+): (a) Von Mises stress distribution, (b) high-stress regions corresponding to observed fracture locations

The penalty of manufacturing-oriented simplification is therefore negligible in absolute terms. Both variants are over-designed, and the 31% stress increase does not change the structural adequacy assessment.

5.2 Manufacturing Metrics Comparison

Table 8 presents full-scale print estimates for ABS material on an Elegoo OrangeStorm Giga printer, comparing both variants across nozzle sizes and infill configurations.

The full-scale boom (∼700 mm) fits within available large-format FDM printers. At matched parameters (ABS, shell, 0.4 mm nozzle), the simplified variant requires 514 g and 131 h versus 568 g and 163 h for the complex variant — a 9.5% reduction in material and 20% reduction in print time. Using a 0.8 mm nozzle reduces print time to 40.5 h but approximately doubles the mass (1039 g), presenting a time-weight trade-off.

The primary manufacturing advantage of the simplified variant is the elimination of support structures on the lower arms. Support structures consume material, extend print time, leave rough surfaces, and create mechanically weak boundary layers [1]. Eliminating supports on the primary structural members addresses all these issues simultaneously and produces smooth bottom surfaces suitable for aerodynamic applications.

5.3 Comparison with Original Composite Boom

Table 9 compares the FDM-printed design with the original carbon fiber tube.

The FDM design is not proposed as a performance-competitive replacement for carbon fiber in weight-critical applications, but as a complementary pathway offering on-demand production, rapid iteration, no minimum order quantities, and accessibility for groups without composite fabrication facilities.

Table 7 Structural performance comparison (full scale, 100% ABS infill)

Metric	Complex	Simplified	Diff.
Mass (100% infill) [kg]	3.351	3.211	−4%
Peak Von Mises stress [MPa]	0.32	0.43	+31%
Peak displ. (boom) [mm]	0.17	0.23	+35%
Peak displ. (full model) [mm]	<1.0	1.25	—
Buckling eigenvalue (load case 1)	43–114	75–266	Simpl. sup.
Buckling eigenvalue (load case 2)	45–113	75–266	Simpl. sup.
Peak stress / UTS ratio	1.2%	1.7%	—
Implied safety factor	>80	∼60	—

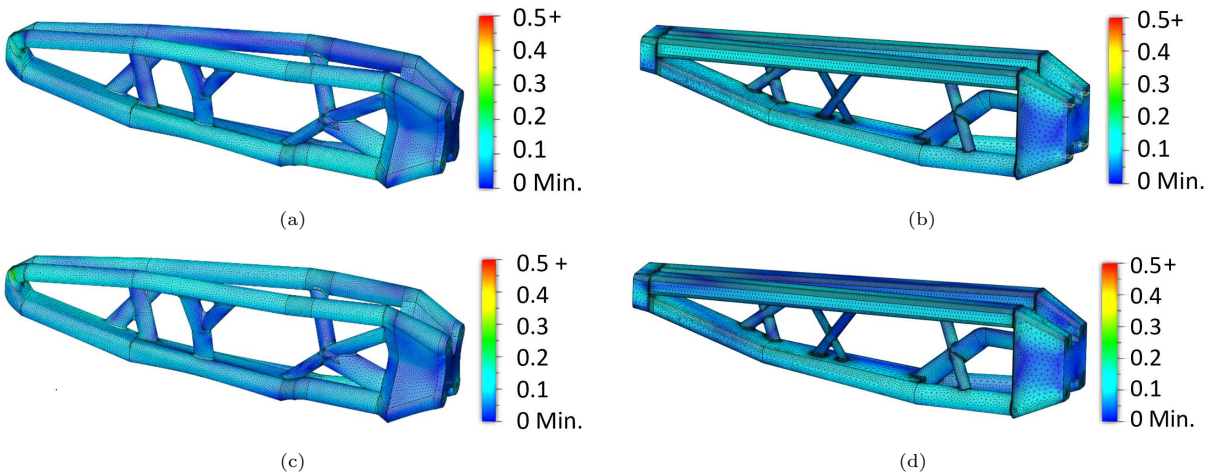


Fig. 13 Von Mises stress comparison: (a) complex, load case 1; (b) simplified, load case 1; (c) complex, load case 2; (d) simplified, load case 2. Scale: 0–0.5 MPa

6 Discussion

6.1 Post-Processing Fidelity and Structural Penalty

Generative design-faithful post-processing offered no meaningful structural advantage over manufacturing-oriented simplification for the tail boom case. Stress levels (0.32–0.43 MPa) are two orders of magnitude below the material limit (25.75 MPa), indicating that structure form is governed by generative design constraints — 4 mm minimum resolution, preserve/obstacle volumes, and mass limit — rather than structural requirements. At safety factors of 60–80, cross-section specifics matter far less than overall topology.

This contrasts with Barbieri and Muzzupappa [5], whose components were designed closer to the structural limit where reconstruction changes had measurable effects. The present case demonstrates that when the output is heavily over-designed — common for polymer FDM parts with high infill — reconstruction fidelity has minimal significance, and resources are better spent on manufacturing-oriented simplification.

Briard et al. [6] described the G-DfAM refinement phase as critical but evaluated it qualitatively. The quantitative evidence here suggests that, for lightly loaded structures, manufacturing-oriented refinement should be the default. A practical guideline: if peak stress in the generative design output is less than 5–10% of the material UTS, aggressive simplification for printability may be justified without detailed structural re-evaluation. For structures approaching the material limit, faithful reconstruction would be more important.

Table 8 Full-scale ABS print estimates (Elegoo OrangeStorm Giga, tree supports, Orca Slicer)

Variant	Infill	Nozzle/Layer [mm]	Mass [g]	Time [h]
Simplified	Shell	0.4 / 0.2	514	131.3
Simplified	15%	0.4 / 0.2	896	179.0
Simplified	Shell	0.8 / 0.4	1039	40.5
Simplified	15%	0.8 / 0.4	1261	45.5
Complex	Shell	0.4 / 0.2	568	163.5
Complex	15%	0.4 / 0.2	949	204.5
Complex	Shell	0.8 / 0.4	1001	43.75
Complex	15%	0.8 / 0.4	1340	51.5

Table 9 Comparison with original carbon fiber tail boom

Attribute	CF tube	FDM simplified
Material	CF composite	ABS
Mass [g]	∼137 (total boom)[a]	514 (total)
Cost per unit	35–76 USD	14–30 USD
Manufacturing method	Specialized	Consumer FDM
Lead time	Supplier-dependent	Hours
Design iteration	New ordering	File modification + reprint
Minimum order	Supplier-dependent	1 unit

[a] Based on measured dimensions (22 mm OD, 18 mm ID) and a 700 mm tube length; carbon fiber tube specifications from manufacturer data.

6.2 FDM Manufacturability Considerations

Eliminating support structures on the lower arms is the most impactful manufacturing change. The complex variant requires 23% more material partly due to supports, which also degrade surface quality and introduce weak interlayer bonds at the support-part interface [1].

Physical test results confirm a secondary optimization opportunity [20, 21]. With safety factors of 60–80 at 100% infill, infill density becomes the primary weight optimization lever. Even the shell-only specimen sustained 12.0 kg — approximately 6 times the design load. A graduated infill approach — higher density at stress concentrations, lower in arm spans — could further reduce mass.

The workflow (generative design in Fusion 360, CAD post-processing, FEA, FDM printing, physical testing) is accessible using only commercial software and consumer-grade printers, suitable for SMEs, research groups, and independent UAV developers seeking to adopt structural optimization [25].

6.3 Limitations and Future Work

Several limitations define directions for future work. Full-scale FEA used ABS properties while physical tests at 40% scale used PLA+ filament; however, the FEA validation at 40% scale (Section 4.2) was performed with PLA+ material properties matching the tested specimens, confirming the model's predictive capability for the tested material. The inter-variant structural comparison (Section 5.1) is material-independent, and PLA+ strength (39.9–52.5 MPa [32]) exceeds the ABS worst-case value used in full-scale FEA, so safety conclusions remain conservative. Scaled prototypes (40%) may not fully represent full-scale behavior, and a single specimen per configuration precludes statistical analysis — though most comparable generative design studies for aerospace [11] and UAV components [13, 15] include no physical testing at all. The isotropic FEA model using worst-case orientation properties provides a conservative estimate, but incorporating fabrication-angle-dependent anisotropy [19]

would improve accuracy. No formal mesh convergence study, dynamic analysis, or fatigue assessment was performed. Future work should address ABS testing at full scale, statistical characterization, anisotropic FEA, and dynamic load assessment.

7 Conclusions

Two post-processing strategies for converting a generative design outcome into an FDM-manufacturable UAV tail boom were compared through FEA and physical load testing — an end-to-end validation that most generative design studies omit.

The manufacturing-oriented (simplified) variant achieved 4% mass reduction and 20% shorter print time compared to the generative design-faithful (complex) variant, while eliminating support structures on the lower arms. The structural cost was a 31% increase in peak Von Mises stress (0.43 vs. 0.32 MPa), yet both values remained below 2% of the material UTS, giving safety factors of 60–80. Buckling resistance was in fact superior in the simplified variant. Physical load testing corroborated the FEA predictions: the solid-infill specimen exceeded 18.15 kg without structural failure, and the shell specimen sustained 12.0 kg before fracture at locations matching FEA-predicted stress concentrations.

These results support a practical guideline: when peak stress in the generative design output is well below the material limit, aggressive simplification for FDM printability is justified without detailed structural re-evaluation. For lightly loaded polymer structures, resources are better spent on support elimination, build orientation optimization, and infill tuning than on faithful reconstruction of the raw topology.

Future work should address full-scale ABS testing, statistical specimen characterization, anisotropic FEA modeling, and dynamic load assessment.

Statements and Declarations

Acknowledgements. The authors wish to thank Przemysław Bibik, Marcin Kasprzyk, Sebastian Topczewski, and Marcin Żugaj for providing the ARCHER platform data that served as input for this study.

Funding. The authors declare that no funds, grants, or other support were received during the preparation of this manuscript.

Competing Interests. The authors have no relevant financial or non-financial interests to disclose.

Author Contributions. M. Kowalik conceived and designed the study, developed the research methodology, supervised the experimental work, and wrote the original manuscript. P. Stapiński conducted the generative design optimization, manufactured the FDM prototypes, performed the mechanical testing, and collected the experimental data. M. Papis contributed to the literature review, co-wrote selected sections, analysed the data, and critically revised the manuscript. All authors read and approved the final version.

Data Availability. The datasets generated and analysed during the current study are available from the corresponding author on reasonable request. CAD models, FEA setup files, and slicer configurations are available upon request.

Use of AI Tools. AI-assisted tools were used for copy editing and language refinement of the manuscript text. The scientific content, data analysis, interpretation, and conclusions are entirely the work of the human authors.

References

[1] Thompson MK, Moroni G, Vaneker T, et al (2016) Design for additive manufacturing: trends, opportunities, considerations, and constraints. CIRP Ann 65:737–760. https://doi.org/10.1016/j.cirp.2016.05.004

[2] Zhu J, Zhou H, Wang C, et al (2021) A review of topology optimization for additive manufacturing: status and challenges. Chin J Aeronaut 34:91–110. https://doi.org/10.1016/j.cja.2020.09.020

[3] Blakey-Milner B, Gradl P, Snedden G, et al (2021) Metal additive manufacturing in aerospace: a review. Mater Des 209:110008. https://doi.org/10.1016/j.matdes.2021.110008

[4] Herzog D, Maiwald MI, Sharma A, et al (2024) Optimization of large-scale aeroengine parts produced by additive manufacturing. In: AIAA SCITECH 2024 Forum, https://doi.org/10.2514/6.2024-1994

[5] Barbieri L, Muzzupappa M (2022) Performance-driven engineering design approaches based on generative design and topology optimization tools: a comparative study. Appl Sci 12:2106. https://doi.org/10.3390/app12042106

[6] Briard T, Segonds F, Zamariola N (2020) G-DfAM: a methodological proposal of generative design for additive manufacturing in the automotive industry. Int J Interact Des Manuf 14:875–886. https://doi.org/10.1007/s12008-020-00669-6

[7] Ibhadode O, Zhang Z, Sixt J, et al (2023) Topology optimization for metal additive manufacturing: current trends, challenges, and future outlook. Virtual Phys Prototyp 18(1):e2181192. https://doi.org/10.1080/17452759.2023.2181192

[8] Zhang L, Li Z, Ying H (2025) Lightweight design process combining generative design and topology optimization based on Fusion 360 and ANSYS: a case study of a biped robot's arch component. Int J Precis Eng Manuf 26(7):1775–1788. https://doi.org/10.1007/s12541-025-01226-5

[9] Regenwetter L, Nobari AH, Ahmed F (2022) Deep generative models in engineering design: a review. ASME J Mech Des 144:071704. https://doi.org/10.1115/1.4053859

[10] Langelaar M (2017) An additive manufacturing filter for topology optimization of print-ready designs. Struct Multidisc Optim 55:871–883. https://doi.org/10.1007/s00158-016-1522-2

[11] Pilagatti AN, Atzeni E, Salmi A (2023) Exploiting the generative design potential to select the best conceptual design of an aerospace component to be produced by additive manufacturing. Int J Adv Manuf Technol 126(11–12):5597–5612. https://doi.org/10.1007/s00170-023-11259-7

[12] Sotomayor NA, Caiazzo F, Alfieri V (2021) Enhancing design for additive manufacturing workflow: optimization, design and simulation tools. Appl Sci 11:6628. https://doi.org/10.3390/app11146628

[13] Balayan A, Mallick R, Dwivedi S, et al (2024) Optimal design of quadcopter chassis using generative design and lightweight materials to advance precision agriculture. Machines 12(3):187. https://doi.org/10.3390/machines12030187

[14] Kowalik M, Śliwiński M, Papis M (2025) Utilization of topology optimization and generative design for drone frame optimization. Aircr Eng Aerosp Technol 97(7):813–823. https://doi.org/10.1108/aeat-12-2024-0384

[15] Maisto G, Garofano A, Acanfora V, et al (2025) Redesigning UAV vertical tail structures with lightweight eco-friendly carbon-reinforced polymers: a generative design-based approach. J Compos Sci 9(10):517. https://doi.org/10.3390/jcs9100517

[16] Yap YL, Toh W, Giam A, et al (2023) Topology optimization and 3D printing of micro-drone: numerical design with experimental testing. Int J Mech Sci 237:107771. https://doi.org/10.1016/j.ijmecsci.2022.107771

[17] Al-Hadithi BM, Alcón Flores S (2025) Design and validation of a 3D-printed drone chassis model through static and transient nonlinear FEM analyses and experimental testing. Drones 9(11):789. https://doi.org/10.3390/drones9110789

[18] Chacón JM, Caminero MÁ, García-Plaza E, et al (2017) Additive manufacturing of PLA structures using fused deposition modelling: effect of process parameters on mechanical properties and their optimal selection. Mater Des 124:143–157. https://doi.org/10.1016/j.matdes.2017.03.065

[19] Sun Z, Guo Y, Shim VPW (2021) Characterisation and modeling of additively-manufactured polymeric hybrid lattice structures for energy absorption. Int J Mech Sci 191:106101. https://doi.org/10.1016/j.ijmecsci.2020.106101

[20] Fernandez-Vicente M, Calle W, Ferrándiz S, et al (2016) Effect of infill parameters on tensile mechanical behavior in desktop 3D printing. 3D Print Addit Manuf 3:183–192. https://doi.org/10.1089/3dp.2015.0036

[21] Lalegani Dezaki M, Mohd Ariffin MKA (2020) The effects of combined infill patterns on mechanical properties in FDM process. Polymers 12(12):2792. https://doi.org/10.3390/polym12122792

[22] Liu J, Yan J, Yu H (2021) Stress-constrained topology optimization for material extrusion polymer additive manufacturing. J Comput Des Eng 8:979–993. https://doi.org/10.1093/jcde/qwab028

[23] Popescu D, Zapciu A, Amza C, et al (2018) FDM process parameters influence over the mechanical properties of polymer specimens: a review. Polym Test 69:157–166. https://doi.org/10.1016/j.polymertesting.2018.05.020

[24] Price M, Zhang W, Friel I, et al (2022) Generative design for additive manufacturing using a biological development analogy. J Comput Des Eng 9(2):463–479. https://doi.org/10.1093/jcde/qwac016

[25] Šostakaitė L, Šapranauskas E, Rudinskas D, et al (2024) Investigating additive manufacturing possibilities for an unmanned aerial vehicle with polymeric materials. Polymers 16(18):2600. https://doi.org/10.3390/polym16182600

[26] Bibik P, Bedńska A, Curyło P, et al (2020) ARCHER – Autonomous Reconfigurable Compound Helicopter for Education and Research. In: 45th European Rotorcraft Forum, Warsaw, Poland, pp 1448–1457, 17–20 September 2019

[27] Żugaj M, Edawdi M, Iwański G, et al (2023) An unmanned helicopter energy consumption analysis. Energies 16(4):2067. https://doi.org/10.3390/en16042067

[28] Fail R, Lawford JA, Eyre RCW (1959) Low-speed experiments on the wake characteristics of flat plates normal to an air stream. Tech. Rep. Reports and Memoranda No. 3120, Aeronautical Research Council, London

[29] Rodriguez-Panes A, Claver J, Camacho AM (2018) The influence of manufacturing parameters on the mechanical behaviour of PLA and ABS pieces manufactured by FDM: a comparative analysis. Materials 11:1333. https://doi.org/10.3390/ma11081333

[30] Zou R, Xia Y, Liu S, et al (2016) Isotropic and anisotropic elasticity and yielding of 3D printed material. Compos Part B Eng 99:506–513. https://doi.org/10.1016/j.compositesb.2016.06.009

[31] Dalpadulo E, Gherardini F, Pini F, et al (2020) Integration of topology optimisation and design variants selection for additive manufacturing-based systematic product redesign. Appl Sci 10(21):7841. https://doi.org/10.3390/app10217841

[32] Hodžić D, Pandžić A, Hajro I, et al (2020) Strength comparison of FDM 3D printed PLA made by different manufacturers. TEM J 9:966–970. https://doi.org/10.18421/TEM93-18